Rebuttal to the concerns raised by the reviewers for the paper titled "A Framework for Dynamic Hyper-local Source Apportionment using Low-cost Sensors for Real-time Policy Action"

(MS No.: egusphere-2025-5677)

Concerns of Reviewer 2:

This manuscript proposes a unique approach for source apportionment of $PM_{2.5}$ via low cost air quality (LCAQ) sensor inputs to machine learning models that are trained via collocated reference grade instruments (RGI). The authors train multi-output regression models from about 7 days of collocated LCAQ/RGI measurements taken at two sites roughly 20 km apart in Lucknow, India, where positive matrix factorization (PMF) is first applied to aerosol mass spectrometer (AMS) and energy dispersive x-ray fluorescence (Xact 625i) measurements and resolved factors serve as the ground truth for model training. Model predictions of AMS and Xact 625i PMF factors are claimed to agree with AMS/Xact 625i PMF factors over 2 day test periods at both sites. As the authors have correctly pointed out, traditional source apportionment (e.g., PMF) of RGI measurements is resource-intensive and often time-consuming. Therefore, their research objectives are timely and relevant to Atmospheric Measurement Techniques, and such a framework proposed would represent an important contribution to the state of the science. However, in its current form, the manuscript lacks the necessary data and methodological rigor to support the objectives or conclusions the authors claim to accomplish. For these reasons, which I detail below, major revisions with additional data and methodological improvements should be made before considering the work for publication.

Concern #1: The work's claims about the proposed framework are disproportionate to the limited training and test data used. Much more RGI/LCAQ data is necessary for the building and evaluating the framework this manuscript is proposing.

The authors describe their framework as robust and effective (e.g. lines 17-18 claim "extensive experimentation done" shows the "robustness of the proposed approach.") yet the employed 80/20 split and very limited test set (2 days of test data) prevent a rigorous evaluation of model performance and the use of AMS/Xact 625i PMF factors as ground truths. PMF factors will vary over time scales much larger than the 10-day windows considered here. It has also been well documented in literature that AMS and Xact 625i PMF factor profiles themselves can vary substantially across sites and, to an extent, even within a site over time (Zhang et al., 2007; Canonaco et al., 2021; Chen et al., 2022). While the framework proposed is interesting, an expanded high-quality dataset is required to demonstrate its potential merit.

In order to demonstrate the need for more data, I pose a few questions to the authors. (a) Because the training set is within 0-7 days of the test set, predicted factor concentrations will already be similar due to autocorrelation – what if the model predicted concentrations a month later or a year later? If periodic RGI/LCAQ relocation periods are required for model training, this would be important information to include. A test set several weeks apart from the training

set would ensure autocorrelation effects are not impacting model performance. (b) In this first submitted manuscript each LCAQ sensor was collocated with the RGI mobile lab and it's my understanding that each regression model is specific to each site. What if the site B model was applied to nearby LCAQ sensor data from site C? This would be another more rigorous evaluation that would show the ability of multi-output regression models to quantify similar sources at a different place and time.

While RGI data and its source apportionment products are resource-intensive, there are many long-term deployments of RGI collocated near LCAQ monitors with free, open-source data products that would be well suited to the models proposed by the authors. For example, the ACTRIS network has aerosol chemical speciation monitors and aethalometers deployed at many sites and has conducted harmonized source apportionment (Chen et al., 2022).

Response: We sincerely thank the reviewer for this thoughtful and constructive comment. We agree that the originally submitted manuscript did not provide sufficient experimental evidence to support broad claims regarding the robustness and generalizability of the proposed framework. The reviewer has correctly emphasized the importance of evaluating the proposed machine learning framework under independent spatial and temporal transfer scenarios.

In response to this important suggestion, we have substantially expanded the experimental evaluation presented in the revised manuscript. Rather than relying only on within-site train-test partitions, the revised study now evaluates the proposed framework under five independent transfer-learning scenarios designed to assess both spatial and temporal generalization.

The principal experiment of the revised manuscript trains the machine learning models using the **combined datasets collected during the October 2023 and February–March 2024 monitoring campaigns at two independent sites in Lucknow (CSIR and BBAU)**. The trained model is subsequently evaluated on an **entirely independent dataset collected during December 2024 at Kanpur**, representing a geographically distinct urban environment. Consequently, the external test data are separated from the earliest training observations by **approximately one year**, thereby substantially reducing the possibility that the reported performance is merely a consequence of short-term temporal autocorrelation.

To further evaluate transferability, four additional transfer-learning experiments have also been incorporated into the revised manuscript:

- **Cross-site transfer:** CSIR → BBAU
- **Cross-site transfer:** BBAU → CSIR
- **Cross-season transfer:** October → February–March
- **Cross-season transfer:** February–March → October

Together, these five experiments assess the robustness of the proposed framework across different monitoring locations, seasonal conditions, and geographical regions.

Furthermore, in response to the reviewer's concern regarding model selection and evaluation, we have revised the complete machine learning workflow. For every transfer-learning experiment, the **source-domain dataset** is partitioned chronologically into **80% training** and **20% validation** subsets (**shuffle = False**), while the **target-domain dataset** is used exclusively as an independent external test set. Hyperparameter optimisation is performed solely on the validation data, after which the selected model is retrained using the combined

training and validation data before being evaluated on the independent test dataset. This revised evaluation protocol eliminates any possibility of information leakage from the external test set during model development.

We agree with the reviewer that evaluation over multiple years and a larger number of cities would provide an even stronger assessment of long-term model robustness. Such an extensive dataset, however, is presently unavailable. Accordingly, we have moderated the claims throughout the revised manuscript and now explicitly present the proposed framework as a **proof-of-concept study** demonstrating the feasibility of real-time source apportionment using calibrated low-cost sensor measurements under independent spatial and temporal transfer scenarios.

We sincerely thank the reviewer for this valuable suggestion. The additional experiments have substantially strengthened the manuscript by providing a significantly more rigorous assessment of the proposed framework under realistic deployment conditions.

The following table shows the revised list of experiments that have been performed and will be included in the revised manuscript.

Experiment	Training Domain	Validation Domain	Independent Test Domain	Purpose
E1	Lucknow (Oct 2023 + Feb–Mar 2024)	20% of Lucknow	Kanpur (Dec 2024)	Cross-city + long-term temporal transfer
E2	CSIR	20% of CSIR	BBAU	Cross-site transfer
E3	BBAU	20% of BBAU	CSIR	Cross-site transfer
E4	October	20% of October	February–March	Cross-season transfer
E5	February–March	20% of February–March	October	Cross-season transfer

Changes to be made in the revised manuscript

- Moderate the claims regarding robustness and generalizability throughout the manuscript.
- Explicitly present the proposed framework as a **proof-of-concept** rather than a universally generalizable framework.
- Include **five transfer-learning experiments** covering:
    - Lucknow → Kanpur (cross-city),
    - CSIR → BBAU,
    - BBAU → CSIR,
    - October → February–March,
    - February–March → October.

- Revise the machine learning methodology to incorporate an **80:20 chronological training–validation split** (**shuffle = False**) together with an **independent external test set**.
- Expand the discussion highlighting that the principal evaluation uses **approximately one year of temporal separation** together with **cross-city validation**, thereby providing a substantially more rigorous assessment than the originally submitted manuscript.

Concern #2: There are concerns about the integrity and reliability of RGI and LCAQ data.

The authors thoughtfully describe the calibration procedure for LCAQ sensors and note the poor agreement between RGI and LCAQ monitors for SO2 and NO2 because measured concentrations are below detection limits. This is especially evident in the Fig. 4 SO2 agreement for site C. The challenges of LCAQ monitors for measuring SO2 and NO2 have been noted extensively (Duvall et al., 2016). If the SO2 and NO2 measurements are not reliable, they should not be included in the machine learning models as they will only impair the model's ability to predict PM2.5 sources.

In Fig. 11, there appears to be poor time resolution or a lack of RGI AMS PMF data and LCAQ PMF predictions within the 2 day test set for site C. Between Oct 8 00:00 and Oct 8 20:00, (about half of the test set) it appears there are only 3 data points being compared. Interestingly, this data appears to be present in Fig. A2. Why does this appear to be excluded in the evaluation in Fig. 11?

Additional information on the operation of the HR-ToF-AMS and Xact 625i should be included in the manuscript. For the HR-ToF-AMS, what were the results of ionization efficiency calibrations? For the Xact 625i, what was the signal-to-noise of the elements measured? For all RGI deployments, what was the inlet height/configuration and position in the mobile lab?

Response: We sincerely thank the reviewer for these valuable observations regarding the reliability of the low-cost sensor measurements and the presentation of the source apportionment results.

Regarding the inclusion of **SO_2** and **NO_2** as predictors, we agree that these channels exhibited comparatively poor calibration performance in the original study. In response to the concerns raised by this reviewer as well as Reviewer 1, we performed a comprehensive re-evaluation of the predictor set. This included (i) additional calibration analyses, (ii) feature ablation studies, and (iii) feature importance analysis using the best-performing Extra Trees regression model.

The additional analyses demonstrated that, for **elemental source apportionment**, the removal of the poorly calibrated predictors (**SO_2**, **NO_2**, and **VOC**) resulted in comparable or slightly improved prediction performance. Consequently, these predictors have been excluded from the

final elemental SA framework in the revised manuscript. The revised elemental model therefore relies only on the more reliable predictors, namely **CO, O_3, $PM_{2.5}$, BC, temperature, relative humidity, and cyclical temporal features**.

For the **organic source apportionment** framework, we revisited both the predictor set and the target representation. The original five-factor PMF solution has been replaced by a chemically more interpretable **three-factor representation (BBOA, HOA and OOA)**. Additional feature importance and feature ablation analyses have been incorporated into the revised manuscript to quantify the contribution of each predictor to the final organic SA model. A detailed discussion of these analyses has been included in our responses to Reviewer 1 (Concerns 3–5).

The reviewer also noted that Figure 11 appeared to contain only a limited number of reference PMF observations between approximately **08 October 00:00 and 08 October 20:00**. We appreciate this careful observation. The apparent reduction in temporal resolution was caused by the limited availability of valid reference PMF observations during portions of the original short-duration test period, rather than by omissions in the machine learning predictions. Consequently, only the available reference observations could be displayed in the original figure.

However, the revised manuscript no longer relies on these original short-duration site-specific experiments. Instead, the complete experimental evaluation has been substantially expanded to include independent **cross-city, cross-site, and cross-season transfer-learning experiments** using considerably larger datasets. The principal evaluation now trains the models using the combined Lucknow datasets collected during the **October 2023** and **February–March 2024** campaigns and evaluates them on an entirely independent dataset collected at **Kanpur during December 2024**. The revised time-series figures therefore contain substantially larger testing datasets and no longer suffer from the visual discontinuities present in the originally submitted manuscript.

We thank the reviewer for these constructive comments, which have led to a substantially more rigorous evaluation framework and a clearer presentation of the revised results.

Further, we thank the reviewer for identifying these missing operational details. We have revised the appendix and section 3.3 to provide additional information on the calibration and operation of the HR-ToF-AMS and Xact 625i, as well as the inlet placement of all research-grade instruments within the mobile laboratory.

HR-ToF-AMS:

Operation: The HR-ToF-AMS (Aerodyne Research Inc., Billerica, MA, USA) was deployed at each campaign site to measure the chemical composition and size-resolved mass concentration of non-refractory $PM_{2.5}$ *at a 2 min time resolution. Ambient aerosol was sampled through a* stainless-steel tubing and a silica-gel diffusion dryer to reduce the influence of humidity. The instrument was operated in V-mode with a vaporizer temperature of approximately 600 °C and an electron-ionization energy of 70 eV. During each measurement cycle, the instrument alternated between mass-spectrum and particle time-of-flight modes, although only mass-spectrum data were used in the present analysis. The data were processed using SQUIRREL in IGOR Pro. A collection efficiency of 1 was applied for the capture vaporizer. Further operational and data-processing details are provided in Decarlo et al., (2006); Lakra et al., (2024); Sethi et al., (2026).

IE Calibration: Key instrumental parameters, including filament current, inlet pressure, turbo-pump temperature, voltages, and flow rate, were monitored daily at each site. Ionization efficiency calibrations were performed at all campaign sites using 300 nm size-selected ammonium nitrate particles and the CPC mass-based method described by Jayne et al., (2000). The resulting IE values were derived from the relationship between the AMS nitrate signal and the nitrate mass concentration calculated from CPC measurements. Further details of the calibration procedure are provided Lakra et al., (2024) and Sethi et al., (2026, preprint). The average ionization efficiency values were 8.67E-08 ions molecule^{-1} at Cycle-1 and 1.05E-07 ions molecule^{-1} at Cycle-2, 1.25E-07 at Kanpur. The calibrations at each site ranged from 1E-08 to 1E-07, indicating stable instrument sensitivity during the campaigns (http://cires.colorado.edu/jimenez-group/UsrMtgs/). These IE calibration results will now be included in the revised appendix and section 2 of the manuscript.

Xact-625i:

Operation: Trace elements were measured at each campaign site using an Xact-625i ambient metals monitor (SailBri Cooper Inc.) operated inside the mobile laboratory at a flow rate of 16.7 L min^{-1} and a 30 min time resolution. The instrument uses energy-dispersive X-ray fluorescence to quantify elemental concentrations collected on a Teflon filter tape. Calibration was performed using NIST-certified thin-film standards, while routine QA/QC included energy alignment, X-ray intensity checks, multi-element standard validation, flow and leak tests, and cyclone cleaning, all within a ±10% tolerance at each site. Further operational details are provided in Lakra et al. (2026).

Signal-to-noise ratio: For the Xact 625i, the analytical signal for each element was evaluated as the ratio of its mean ambient concentration to the corresponding 30-min method detection limit (MDL) (Table R1). This ratio indicates the strength of the measured elemental signal relative to the minimum detectable concentration. Ratios greater than 3 indicate that the mean concentrations were sufficiently above the detection limit, whereas ratios close to or below 1 indicate weak signals that were near or below the instrumental detection capability (Kadachi and Al-eshaikh, 2012). During Campaign I, the concentration-to-MDL ratios ranged from 0.02 to 584.48 at CSIR-CIMAP and from 0.01 to 837.94 at BBAU. During Campaign II, the corresponding ratios ranged from 0.01 to 464.09 at CSIR-CIMAP and from 0.02 to 997.82 at BBAU. At Kanpur, the ratios ranged from 0.17 to 1322.55. The wide range reflects substantial differences in ambient concentrations among the measured elements. Elements such as S, K, Ca, Ti, Fe, Cu, Zn, Br, and Pb exhibited high ratios, indicating strong and consistently detectable signals. In contrast, elements such as Al, V, Co, Mo, Cd, In, Sn, Sb, and Bi generally showed low ratios, indicating that their concentrations were frequently close to or below the MDL. However, some elements with lower ratios, such as V, Se, Ba, Rb, and Cr, were retained in the PMF analysis because of their importance as source markers (Table R1).

Table R1.1. Average concentration of each trace element (ng/m³) at each site in C-I, C-II, and Kanpur with MDL and S/N ratio.

Trace element	MDL (30 min)	C-I CIMAP Mean (ng/m³)	C-I BBAU Mean (ng/m³)	C-I CIMAP S/N	C-I BBAU S/N	C-II CIMAP Mean	C-II BBAU Mean (ng/m³)	C-II CIMAP S/N	C-II BBAU S/N	Kanpur Mean (ng/m³)	Kanpur S/N
Si	89	649.35	833.61	7.3	9.37	727.65	1293.4	8.18	14.53	1392.19	15.64

S	16	2744.8	2758.6	171.5	172.4	2632.1	3012.7	164.5	188.2	6156.4	384.78
Cl	8.6	169.60	375.09	19.72	43.62	1703.6	1260.1	198.1	146.5	7910.5	919.83
K	5.8	1226.63	1596.41	211.5	275.2	1711.5	1916.8	295.1	330.49	3866.25	666.6
Ca	1.5	320.17	396.5	213.45	264.33	331.89	445.1	221.26	296.73	1139.69	759.79
Ti	0.79	28.64	39.03	36.25	49.41	29.17	40.61	36.92	51.41	64.95	82.22
V	0.6	0.75	0.57	1.25	0.95	0.36	0.56	0.6	0.93	0.8	1.34
Cr	0.58	2.70	5.38	4.66	9.28	1.41	1.61	2.43	2.78	9	15.53
Mn	0.71	8.02	20.52	11.3	28.9	9.28	10.01	13.07	14.1	43.52	61.3
Fe	0.85	329.10	451.44	387.18	531.11	339.43	478.43	399.33	562.86	894.18	1051.97
Ni	0.47	1.39	0.98	2.96	2.09	0.52	0.87	1.11	1.85	2.4	5.1
Cu	0.39	11.85	12.16	30.38	31.18	11.93	10.07	30.59	25.82	44.69	114.59
Zn	0.33	192.88	276.52	584.48	837.94	153.15	329.28	464.09	997.82	436.44	1322.55
As	0.31	2.98	2.31	9.61	7.45	2.01	1.78	6.48	5.74	11.13	35.92
Se	0.4	1.43	1.1	3.58	2.75	1.83	1.93	4.58	4.83	4.02	10.04
Br	0.52	9.88	12.61	19	24.25	24.69	25.8	47.48	49.62	60.71	116.75
Rb	0.95	0.97	1.28	1.02	1.35	1.8	2.41	1.89	2.54	6.89	7.25
Sr	1.1	2.16	2.48	1.96	2.25	2.99	2.63	2.72	2.39	5.52	5.02
Ba	1.9	0.62	2.27	0.33	1.19	6.05	0.7	3.18	0.37	8.66	4.56
Pb	0.63	57.50	76.58	91.27	121.56	47.15	53.23	74.84	84.49	351.65	558.17

Mobile Van Inlets: The inlets were mounted on the van's rooftop during stationary measurements. The HR-ToF-AMS, Xact 625i, EBAM, AE-51, Gas Analysers and other instruments were installed inside the temperature-controlled mobile laboratory and connected to independent roof-mounted sampling inlets. For most of the instruments, the inlets are straight to reduce any particle loss (Chow, 1995). The relative positions of the instruments and inlet devices are illustrated in Figure R2.1 (taken from study Lakra et al. (2026)).

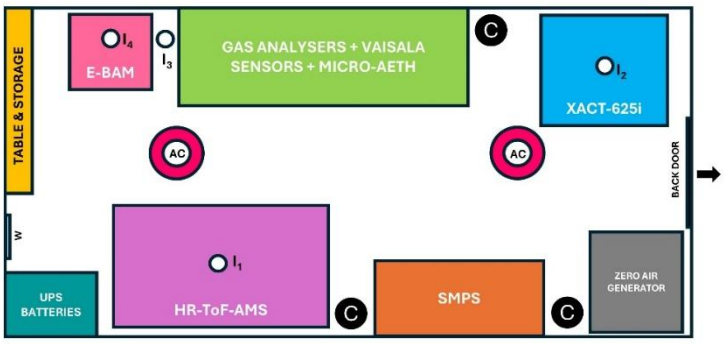

Fig. R2.1. Position of different instruments equipped inside the mobile laboratory. I1 (HR-ToF-AMS and SMPS), I2 (Xact-625i), I3 (gas analyzer, micro-Aeth, and Vaisala sensors), and I4 (E-BAM) represent the sampling inlets from the rooftop. C shows the 3 cylinders (NOx, SOx, CO) for gas analyser calibration. W shows the window, and AC represents air conditioners (Fig. S2 from study Lakra et al. (2026)).

Changes to be made in the revised manuscript:

- All the details will be revised in Section 2 and the appendix of the manuscript, including a new table of S/N ratios.

Concern #3: The PMF source factors are being overinterpreted, and additional details should be provided on PMF source apportionment methods.

From 20 days of HR-ToF-AMS and Xact 625i measurements, the authors have resolved 5 AMS source factors and 7 Xact 625i source factors and claim the model is able to predict these different source factors well. Some of the PMF factors (e.g., "Fe-smelting") seem very specific considering that other large sources of particulate iron exist (e.g., brake wear). The manuscript needs a more thorough rationalization of the PMF solutions (e.g., correlations with external tracers, diurnal profiles, comparisons to prior literature, bootstrapping). If the RGI PMF factors themselves have a high degree of uncertainty and mixing, I would not expect the LCAQ sensors to predict such factors well. If the model is not able to reproduce accurate source apportionment of these 12 factors with an expanded dataset, I would advise the authors to consider applying the model to simpler groups first (e.g., hydrocarbon like organic aerosol, oxygenated organic aerosol, sulfate, nitrate).

Response: We thank the reviewer for this important comment. In response, we substantially expanded the PMF input dataset beyond the original approximately 20-day measurement period by including additional C-II datasets from CSIR-CIMAP and BBAU, conducted from February to March 2024, along with the Kanpur measurements conducted in December 2025. The total number of days has now increased to 63. The PMF analyses were repeated using the expanded dataset, which provided more stable and similar factor solutions.

The revised HR-ToF-AMS analysis resolved five factors: HOA, BBOA-I, BBOA-II, SVOOA, and LVOOA, while the Xact 625i analysis resolved seven factors: S-rich, Cl-rich, Dust, Non-Exhaust, SFC-I, SFC-II, and Pb-rich. The previously identified, highly source-specific "Fe-smelting" factor was not reproduced in the expanded analysis. Including additional sites and campaign periods increased the number of observations and introduced greater spatial, temporal, and source variability, thereby reducing the influence of short-duration or site-specific Fe-rich episodes on the PMF solution. Instead of forming a distinct factor, Fe was distributed mainly among the Dust and Non-Exhaust factors together with other crustal and traffic-related metals. This indicates that the earlier "Fe-smelting" assignment was insufficiently robust as a unique source and likely reflected mixed Fe-rich emissions in the shorter dataset.

A detailed interpretation and justification of the resolved factors, including their chemical profiles, characteristic tracers, diurnal variations, correlations with external measurements, and stability assessments, are provided in our related mobile-lab studies from the same sites. The HR-ToF-AMS factors are discussed in detail in Sethi et al. (2026, under review) while the Xact 625i factors and their source interpretation are described in (Lakra et al., 2026). Therefore, only a concise summary of the factor characteristics, Q/Qexp, external correlation and bootstrap assessment has been included in the revised supplementary information of the manuscript, with appropriate references to these studies.

PMF input matrices and selection of the optimum solutions

For the **HR-ToF-AMS** analysis, the unit-mass-resolution (UMR) organic mass spectra were processed using SQUIRREL after removing spectra affected by instrument malfunction, calibration issues, or other invalid runs. The remaining data were averaged to a 30-minute resolution and used to construct the concentration and corresponding error matrices. The final AMS input matrix contained 2142 observations and 300 (m/z) variables. The large number of valid observations relative to the number of variables provided sufficient temporal variability and degrees of freedom for resolving the five-factor solution.

For the **Xact-625i** analysis, the 30-minute elemental concentration and uncertainty datasets were aligned across all included deployments. Elements with a detection limit below MDL were excluded. The final Xact input matrix contained 2424 observations and 21 elemental variables. The expanded multi-site dataset included substantially more observations than the original analysis and captured variations across sites, seasons, meteorological conditions, and source environments.

Solutions with different numbers of factors were examined for both datasets. The 5-factor AMS and 7-factor Xact solutions were selected based on changes in Q/Qexp, factor-profile interpretability, temporal behaviour, external-tracer relationships, and factor stability (Fig. R2.2). For the AMS analysis, the 5-factor solution was selected because we observed the maximum Q/Qexp relative change from 4 to 5 factors, whereas the 7-factor Xact solution shows the maximum Q/Qexp relative change from 6 to 7 factors. Adding further factors primarily splits physically meaningful factors, whereas solutions with fewer factors showed mixing of chemically distinct source profiles (Fig. R2.2).

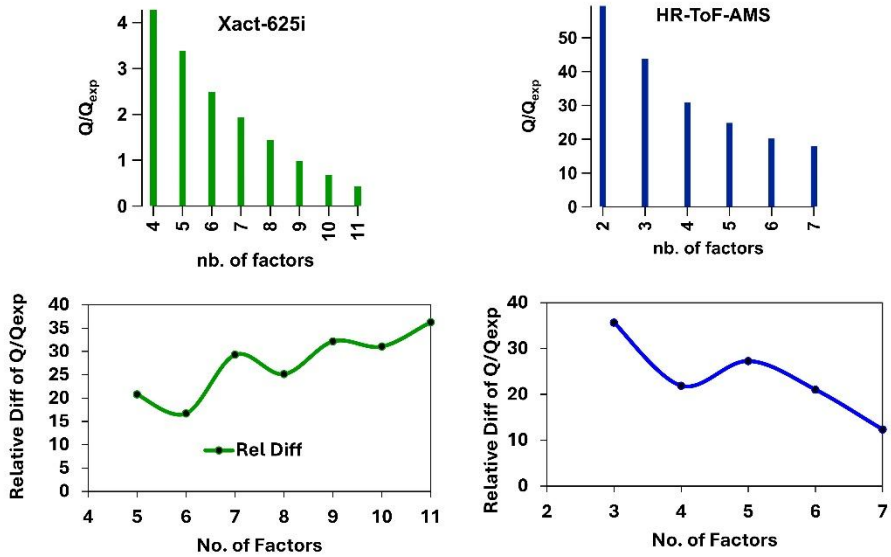

Figure R2.2: Q/Qexp and its relative difference (%) plot with respect to the number of factors for optimum PMF solution selection criteria of elemental SA (Xact-625i) and Organics SA (HR-ToF-AMS)

Bootstrap assessment

To evaluate the stability of the PMF solutions, 1000 bootstrap resampling runs were performed in SoFi using criterion-based selection. The final five-factor AMS and seven-factor Xact solutions, with all factors unconstrained, were used as the base cases. Bootstrapped factors were mapped using an active Pearson correlation criterion ($R > 0.9$), and only valid, unmixed runs were retained. Overall, 857 runs (85.7%) for AMS and 923 runs (92.3%) for Xact were successfully mapped, indicating good factor stability and reproducibility.

Brief interpretation of the HR-ToF-AMS factors:

HOA: As a primary organic aerosol (POA) factor, HOA was characterized by hydrocarbon fragments at m/z 41, 43, 55, 57, 69, and 71, together with the aromatic fragment at $m/z131$ and low contributions from oxygenated ions (Fig. R2.3). These fragments are associated with fresh traffic and fossil-fuel combustion emissions (Tobler et al., 2020). It's morning, and evening peaks were consistent with the traffic peak hour and the accumulation of primary emissions under a shallow boundary layer. HOA contributed 13% of the total organic aerosol and showed a good correlation with black carbon (BC) (R = 0.65), further supporting its association with vehicle exhaust (Shukla et al., 2021a) (Figs. R2.3, R2.5). HOA was highest at BBAU during Cycle-II, followed by Kanpur, consistent with its proximity to major traffic corridors and meteorological conditions that favoured pollutant accumulation. The high HOA in Kanpur was attributed to nearby commercial activity, traffic intersections, and frequent vehicular movement.

BBOA-I: BBOA-I was also identified as a primary organic aerosol factor with low contribution from m/z44 (oxygenated ion) and contributed 12% of the total organic aerosol. Its mass spectrum was characterized by the biomass-burning marker ions at m/z 60 and 73, together with hydrocarbon and aromatic fragments (m/z 178, 202), indicating relatively fresh biomass and solid fuel combustion emissions (Goetz et al., 2022) (Fig. R2.3). Its diurnal profile showed high concentrations during the late evening, nighttime, and early morning, with a pronounced increase after approximately 19:00 and minimum concentrations during the afternoon. This pattern is consistent with nighttime biomass burning or domestic solid-fuel burning and the accumulation of primary emissions under reduced boundary-layer mixing. BBOA-I was highest at Kanpur, likely due to wintertime biomass and solid-fuel burning for domestic heating, followed by BBAU during Cycle I, where post-monsoon agricultural-residue burning may have contributed (Fig. R2.3). The lowest concentrations were observed at CSIR-CIMAP, reflecting its background nature and limited nearby combustion sources. Its correlations with Chl (R = 0.57) and BC (R = 0.67) further supported its combustion-related origin (Lalchandani et al., 2022) (Fig. R2.5).

BBOA-II: BBOA-II contributed 14% of the total organic aerosol and was identified as a more oxidized biomass-burning factor. Its mass spectrum retained the characteristic biomass-burning fragments at m/z 60 and 73 but showed a stronger contribution at m/z 44, indicating atmospheric ageing and secondary organic aerosol (SOA) formation (Lalchandani et al., 2022). Its diurnal profile exhibited a morning peak around 09:00–10:00, following the earlier BBOA-I increment, suggesting oxidation of freshly emitted biomass-burning aerosol (Fig. R2.3). An increase during nighttime may be associated with oxidation by NO_3 radicals under stable atmospheric conditions (Lakra et al., 2024). BBOA-II was highest at Kanpur during winter, followed by BBAU during Cycle I and CSIR-CIMAP during Cycle II, reflecting differences in biomass-burning emissions and atmospheric processing across the sites.

SVOOA: SVOOA contributed 20% of the total organic aerosol and was characterized by oxygenated fragments at m/z 44, together with smaller contributions from less-oxidized hydrocarbon ions (Manchanda et al., 2021) (Fig. R2.3). This composition indicates partially oxidized and comparatively semi-volatile organic aerosol. Its concentration increased during the late morning, consistent with photochemical oxidation of locally emitted precursors under sunlight (Li et al., 2013). SVOOA was highest in Kanpur, possibly because stronger local wintertime emissions provided abundant precursors that underwent initial atmospheric ageing. It shows good correlation with nitrate (R=0.51), further suggesting a secondary nature (Fig. R2.5).

LVOOA: LVOOA was the dominant AMS factor, contributing 41% of the total organic aerosol. Its mass spectrum showed the strongest oxygenated signature, particularly a high relative abundance of $m/z44$, consistent with highly aged and low-volatility secondary organic aerosol (Li et al., 2013) (Fig. R2.3). Its concentration increased during the afternoon, following the rise in SVOOA, indicating continued photochemical ageing and transformation of semi-volatile into more oxidized, lower-volatility species. LVOOA was the largest contributor at each site and showed a comparatively higher concentration at CSIR-CIMAP than other factors, supporting the influence of regionally transported and aged aerosol at this background location. It shows a good correlation with sulfate (R=0.56), supporting its secondary nature (Guo et al., 2020) (Fig. R2.5).

Brief interpretation of the Xact 625i factors

S-rich: The S-rich factor contributed 32% of the total elemental mass and was dominated by S (85.7%), followed by K (12.2%) (Shukla et al., 2023) (Fig. R2.4). It shows a relatively flat diurnal profile, indicating a secondary source rather than a direct local emission. The moderate correlation with AMS sulfate (R = 0.51) further supports this. Sulfur released mainly as SO_2 from coal and other combustion activities can undergo gas-phase and aqueous-phase oxidation to form particulate sulfate. The associations with K (R = 0.53) likely reflect the combustion origin of the precursor emissions (Sharma and Mandal, 2023) (Fig. R2.5). S-rich was highest at Kanpur, followed by the Lucknow Cycle-II sites, and was lowest at CSIR-CIMAP during Cycle I. The higher Kanpur concentration likely reflects stronger combustion-related SO_2 emissions from the nearby Panki power plant and subsequent sulfate formation, whereas the lower concentration at CSIR-CIMAP is consistent with its background nature.

Cl-rich: The Cl-rich factor contributed 23% of the total elemental mass and was dominated by Cl (80.6%), followed by S (12.1%) and K (4.3%) (Fig. R2.4) (Lakra et al., 2026). It showed a pronounced morning peak, a strong daytime decline, and a slight evening increase, consistent with fresh combustion emissions followed by dilution and volatilization of particulate chloride. Its strong correlation with AMS chloride ($R = 0.82$) and K ($R = 0.70$), together with moderate correlations with Rb, Br, As, and Cu, supports contributions from biomass, solid-fuel, and waste-burning emissions (Shukla et al., 2021a) (Fig. R2.5). Cl-rich was highest at Kanpur, followed by the Lucknow Cycle-II sites, and lowest at CSIR-CIMAP during Cycle I. The elevated Kanpur concentration likely reflects stronger wintertime solid-fuel and waste-burning activities.

Dust: The Dust factor was dominated by Si (48.6%), Ca (24.2%), and Fe (19.9%), with smaller contributions from K and Ti and contributed 18% of the total elemental mass (Rai et al., 2020) (Fig. R2.4). Its gradual daytime increase and evening peak indicate dust resuspension

associated with traffic. Strong correlations with Fe (R = 0.87), Mn (R = 0.63), and Cr (R = 0.51) suggest that the factor includes both crustal material and traffic-contaminated road dust (Lakra et al., 2026) (Fig. R2.5). Dust was highest at Kanpur, followed by BBAU during Cycle II, and lowest at CSIR-CIMAP during Cycle I. The higher concentrations at Kanpur and BBAU likely reflect higher traffic-induced resuspension.

SFC-I: The SFC-I factor was dominated by K (90.8%), followed by S (6.0%) (Fig. R2.4). Its morning and evening enhancements, together with strong correlations with K (R = 0.96), Rb (R = 0.81), BC (R = 0.54), and AMS Chl (R = 0.54), support emissions from biomass and other solid-fuel combustion (Rai et al., 2021) (Figs. R2.4, R2.5). It contributed 15% of the total elemental mass and was highest at Kanpur, followed by BBAU, likely due to wintertime domestic heating and local combustion.

SFC-II: The SFC-II factor contributed the lowest with 3% and was dominated by Zn (72.5%), followed by S (17.1%), Fe (5.6%), and Si (4.4%) (Shukla et al., 2021b) (Fig. R2.4). It showed a modest morning enhancement and weaker associations with Fe (R = 0.39) and Mn (R = 0.31), indicating mixed Zn-rich emissions from solid fuels, waste burning, traffic, or industry (Fig. R2.5). Episodic peaks were most pronounced at BBAU, particularly during Cycle II, followed by Kanpur, whereas CSIR-CIMAP showed the lowest concentrations.

Non-Exhaust: The Non-Exhaust factor was dominated by Fe (43.9%), Si (28.6%), Mn (10.6%), and Ca (5.9%), with smaller contributions from Cu and Zn (Fig. R2.4). It contributed 6% of the total elemental mass. The diurnal variations show morning and evening increments, which were consistent with traffic activity and road-dust resuspension. Strong correlations with Fe (R=0.82), Mn (R=0.80), Cr (R=0.49), and BC (Lakra et al., 2026) (R=0.45) support contributions from brake wear, mechanical abrasion, and traffic-related resuspended dust (Fig. R2.5). It was highest at Kanpur, followed by BBAU during Cycle II, and lowest at CSIR-CIMAP during Cycle I, reflecting differences in traffic intensity and local road activity.

Pb-rich: The Pb-rich factor contributed 3% of the total elemental mass and was dominated by S (44.9%) and Pb (27.1%), followed by K (12.9%) and Cl (6.2%) (Fig. R2.4). Its strong correlations with As (R=0.82) and Se (R=0.65) indicate coal-combustion emissions (Li et al., 2012) (Fig. R2.5). The factor showed weak diurnal variation with occasional short-duration peaks, suggesting intermittent local sources. Pb-rich concentrations were highest at Kanpur due to the combustion of coal during the winter for heating purposes. It also reflects a stronger influence from commercial, combustion, waste-burning, or metal-related activities at the more urban sites.

Overall, the revised factors are supported by their characteristic profiles, temporal and diurnal behaviour, relative mass contributions, and relationships with external tracers. We have avoided assigning factors to highly specific industries when the marker species can arise from multiple sources. The revised manuscript therefore describes them as broad PMF-resolved chemical or source-related factors rather than unique emission sources. Detailed factor profiles, diurnal variations, external correlations, and bootstrap results have been added to Figures of the revised Supplementary Information.

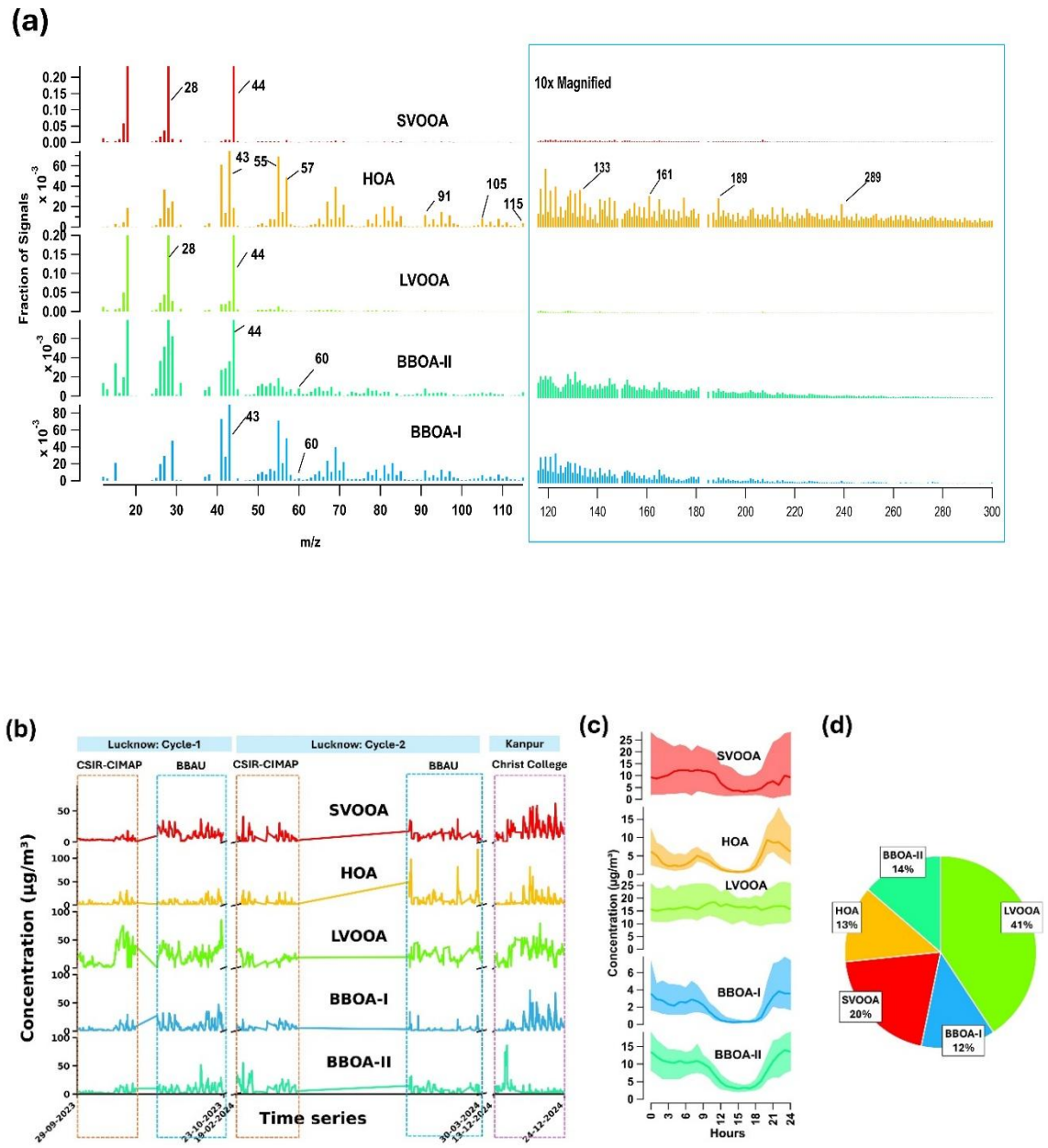

Figure R2.3. (a) m/z spectra for the different organic factors during the measurement period, (b) Time series plots (c) Diurnal (d) Fractional contribution for the different PMF resolved factors of organic aerosol.

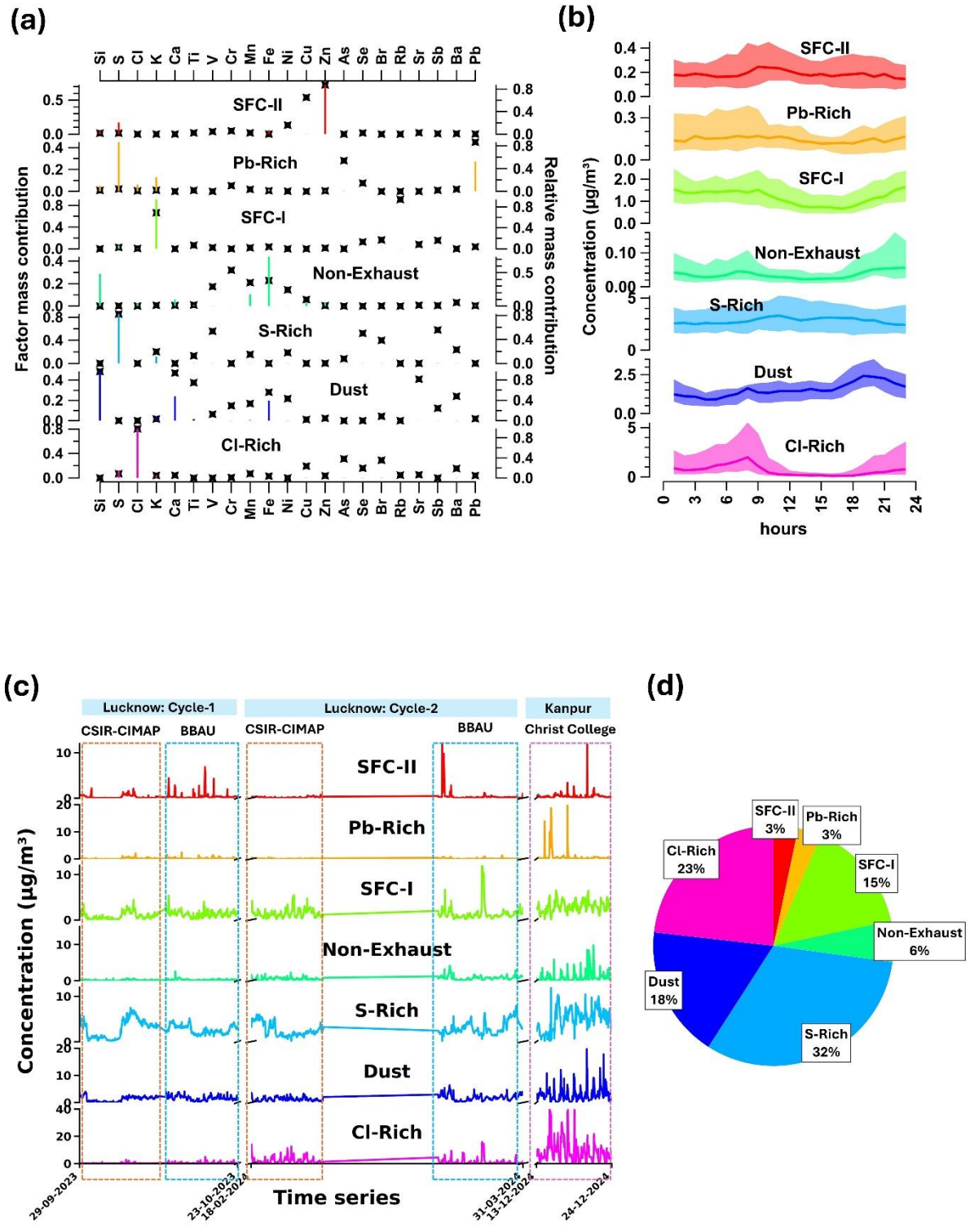

Figure R2.4. (a) Spectra profile for the different elemental factors during the measurement period, (b) Diurnal, (c) Time series plots, (d) Fractional contribution for the different PMF resolved factors of Trace elements.

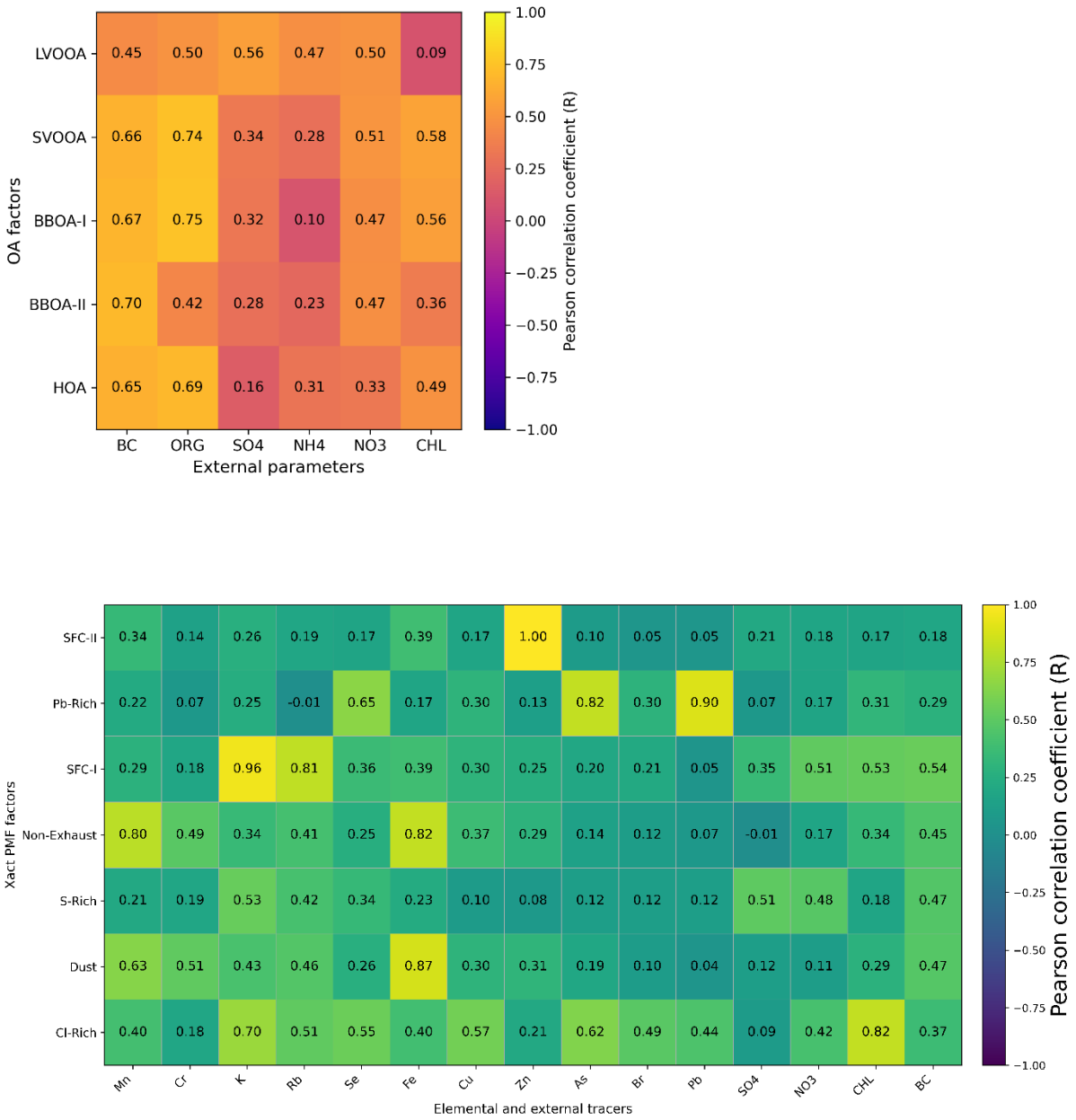

Figure R2.5. Heatmap between (a) PMF resolved OA sources and external parameters, and (b) PMF resolved elemental sources and external parameters.

Changes to be made in revised manuscript:

- All the details of RTSA will be revised in the appendix of the manuscript, including a new and modified figure.

References:

Chow, J.C., 1995. Measurement methods to determine compliance with ambient air quality standards for suspended particles. J. Air Waste Manag. Assoc. 45, 320–382. https://doi.org/10.1080/10473289.1995.10467369

Decarlo, P.F., Kimmel, J.R., Trimborn, A., Northway, M.J., Jayne, J.T., Aiken, A.C., Gonin, M., Fuhrer, K., Horvath, T., Docherty, K.S., Worsnop, D.R., Jimenez, J.L., 2006. Field-deployable, high-resolution, time-of-flight aerosol mass spectrometer. Anal. Chem. 78, 8281–8289. https://doi.org/10.1021/ac061249n

DeCarlo, P.F., Kimmel, J.R., Trimborn, A., Northway, M.J., Jayne, J.T., Aiken, A.C., Gonin, M., Fuhrer, K., Horvath, T., Docherty, K.S., Worsnop, D.R., Jimenez, J.L., 2006. Field-deployable, high-resolution, time-of-flight aerosol mass spectrometer. Anal. Chem. 78, 8281–8289. https://doi.org/10.1021/ac061249n

Goetz, J.D., Giordano, M.R., Stockwell, C.E., Bhave, P. V, Puppala, P.S., Panday, A.K., Jayarathne, T., Stone, E.A., Yokelson, R.J., Decarlo, P.F., 2022. Aerosol Mass Spectral Profiles from NAMaSTE Field-Sampled South Asian Combustion Sources. Environ. Sci. Technol. https://doi.org/10.1021/acsearthspacechem.2c00173

Guo, J., Zhou, S., Cai, M., Zhao, J., Song, W., Zhao, W., Hu, W., Sun, Y., He, Y., Yang, C., Xu, X., Zhang, Z., Cheng, P., Fan, Q., Hang, J., Fan, S., Wang, Xinming, Wang, Xuemei, 2020. Characterization of submicron particles by time-of-flight aerosol chemical speciation monitor (ToF-ACSM) during wintertime: Aerosol composition, sources, and chemical processes in Guangzhou, China. Atmos. Chem. Phys. 20, 7595–7615. https://doi.org/10.5194/acp-20-7595-2020

Jayne, J.T., Leard, D.C., Zhang, X., Davidovits, P., Smith, K.A., Kolb, C.E., Worsnop, D.R., 2000. Development of an aerosol mass spectrometer for size and composition analysis of submicron particles. Aerosol Sci. Technol. 33, 49–70. https://doi.org/10.1080/027868200410840

Kadachi, A.N., Al-eshaikh, M.A., 2012. Limits of detection in XRF spectroscopy. X-Ray Spectrom. 350–354. https://doi.org/10.1002/xrs.2412

Lakra, A., Kumar, A., Sethi, D., Sekhar, H., Jain, V., Tripathi, S.N., 2026. High-resolution source apportionment and health risks of PM 2 . 5 -bound trace elements across a major Indian city : Seasonal and diurnal insights from a multi-site campaign using a mobile laboratory platform. Atmos. Environ. 365, 121675. https://doi.org/10.1016/j.atmosenv.2025.121675

Lakra, A., Shukla, A.K., Bhowmik, H.S., Yadav, A.K., Jain, V., Murari, V., Gaddamidi, S., Lalchandani, V., Tripathi, S.N., 2024. Comparative analysis of winter composite-PM2.5 in Central Indo Gangetic Plain cities: Combined organic and inorganic source apportionment and characterization, with a focus on the photochemical age effect on secondary organic aerosol formation. Atmos. Environ. 338, 120827. https://doi.org/10.1016/j.atmosenv.2024.120827

Lalchandani, V., Srivastava, D., Dave, J., Mishra, S., Tripathi, N., Shukla, A.K., Sahu, R., Thamban, N.M., Gaddamidi, S., Dixit, K., Ganguly, D., Tiwari, S., Srivastava, A.K., Sahu, L., Rastogi, N., Gargava, P., Tripathi, S.N., 2022. Effect of Biomass Burning on PM2.5 Composition and Secondary Aerosol Formation During Post-Monsoon and Winter Haze Episodes in Delhi. J. Geophys. Res. Atmos. 127.

https://doi.org/10.1029/2021JD035232

Li, Q., Cheng, H., Zhou, T., Lin, C., Guo, S., 2012. The estimated atmospheric lead emissions in China, 1990-2009. Atmos. Environ. 60, 1–8. https://doi.org/10.1016/j.atmosenv.2012.06.025

Li, Y.J., Lee, B.Y.L., Yu, J.Z., Ng, N.L., Chan, C.K., 2013. Evaluating the degree of oxygenation of organic aerosol during foggy and hazy days in Hong Kong using high-resolution time-of-flight aerosol mass spectrometry (HR-ToF-AMS). Atmos. Chem. Phys. 13, 8739–8753. https://doi.org/10.5194/acp-13-8739-2013

Manchanda, C., Kumar, M., Singh, V., Faisal, M., Hazarika, N., Shukla, A., Lalchandani, V., Goel, V., Thamban, N., Ganguly, D., Tripathi, S.N., 2021. Variation in chemical composition and sources of PM2.5 during the COVID-19 lockdown in Delhi. Environ. Int. 153, 106541. https://doi.org/10.1016/j.envint.2021.106541

Rai, P., Furger, M., El Haddad, I., Kumar, V., Wang, L., Singh, A., Dixit, K., Bhattu, D., Petit, J.E., Ganguly, D., Rastogi, N., Baltensperger, U., Tripathi, S.N., Slowik, J.G., Prévôt, A.S.H., 2020. Real-time measurement and source apportionment of elements in Delhi's atmosphere. Sci. Total Environ. 742. https://doi.org/10.1016/j.scitotenv.2020.140332

Rai, P., Slowik, J.G., Furger, M., El Haddad, I., Visser, S., Tong, Y., Singh, A., Wehrle, G., Kumar, V., Tobler, A.K., Bhattu, D., Wang, L., Ganguly, D., Rastogi, N., Huang, R.J., Necki, J., Cao, J., Tripathi, S.N., Baltensperger, U., Prevot, A.S.H., 2021. Highly time-resolved measurements of element concentrations in PM10 and PM2.5: Comparison of Delhi, Beijing, London, and Krakow. Atmos. Chem. Phys. 21, 717–730. https://doi.org/10.5194/acp-21-717-2021

Sethi, D., Lakra, A., Kumar, A., Chakraborty, S., Sekhar, H., Jain, V., Tripathi, S.N., 2026. Hyperlocal air quality monitoring and source apportionment of non- refractory $PM_{2.5}$ at three urban sites using stationary van - based measurements : A Lucknow case study. Atmos. Chem. Phys. 1–41. https://doi.org/10.5194/egusphere-2026-595

Sharma, S.K., Mandal, T.K., 2023. Elemental Composition and Sources of Fine Particulate Matter (PM2.5) in Delhi, India. Bull. Environ. Contam. Toxicol. 110, 1–8. https://doi.org/10.1007/s00128-023-03707-7

Shukla, A.K., Lalchandani, V., Bhattu, D., Dave, J.S., Rai, P., Thamban, N.M., Mishra, S., Gaddamidi, S., Tripathi, N., Vats, P., Rastogi, N., Sahu, L., Ganguly, D., Kumar, M., Singh, V., Gargava, P., Tripathi, S.N., 2021a. Real-time quantification and source apportionment of fine particulate matter including organics and elements in Delhi during summertime. Atmos. Environ. 261, 118598. https://doi.org/10.1016/j.atmosenv.2021.118598

Shukla, A.K., Lalchandani, V., Bhattu, D., Dave, J.S., Rai, P., Thamban, N.M., Mishra, S., Gaddamidi, S., Tripathi, N., Vats, P., Rastogi, N., Sahu, L., Ganguly, D., Kumar, M., Singh, V., Gargava, P., Tripathi, S.N., 2021b. Real-time quantification and source apportionment of fine particulate matter including organics and elements in Delhi during summertime. Atmos. Environ. 261. https://doi.org/10.1016/j.atmosenv.2021.118598

Shukla, A.K., Tripathi, S.N., Canonaco, F., Lalchandani, V., Sahu, R., Srivastava, D., Dave, J., Thamban, N.M., Gaddamidi, S., Sahu, L., Kumar, M., Singh, V., Rastogi, N., 2023. Spatio-temporal variation of C-PM2.5 (composition based PM2.5) sources using PMF*PMF (double-PMF) and single-combined PMF technique on real-time non-

refractory, BC and elemental measurements during post-monsoon and winter at two sites in Delhi, India. Atmos. Environ. 293, 119456. https://doi.org/10.1016/j.atmosenv.2022.119456

Tobler, A., Bhattu, D., Canonaco, F., Lalchandani, V., Shukla, A., Thamban, N.M., Mishra, S., Srivastava, A.K., Bisht, D.S., Tiwari, S., Singh, S., Močnik, G., Baltensperger, U., Tripathi, S.N., Slowik, J.G., Prévôt, A.S.H., 2020. Chemical characterization of PM2.5 and source apportionment of organic aerosol in New Delhi, India. Sci. Total Environ. 745. https://doi.org/10.1016/j.scitotenv.2020.140924